ELSEVIER

Journal of Structural Geology 28 (2006) 9–18

JOURNAL OF STRUCTURAL GEOLOGY

www.elsevier.com/locate/jsg

Anisotropy of magnetic susceptibility (AMS) analysis of basalt dikes at Cathedral Cliffs, WY: implications for Heart Mountain faulting

Josh DeFrates[a], David H. Malone[a,*], John P. Craddock[b]

[a]*Department of Geography-Geology, Illinois State University, Campus Box 4400, Normal, IL 61790-4400, USA*
[b]*Geology Department, Macalester College, St Paul, MN 55105, USA*

Received 8 April 2005; received in revised form 13 September 2005; accepted 15 September 2005
Available online 2 November 2005

Abstract

Mafic dikes pervade the upper plate of the Heart Mountain Detachment (HMD), yet the dike concentration in the lower plate is sparse. Previous workers interpreted that these dikes were emplaced either coeval with or subsequent to the emplacement of the upper plate. The magnetic fabrics of 32 mafic dikes at Cathedral Cliffs were analyzed using low-field anisotropy of magnetic susceptibility (AMS) as a proxy for flow. These dikes intrude Ordovician–Mississippian carbonate and overlying Eocene volcanic rocks and are truncated along the nearly horizontal HMD. The dikes trend between N10°W and N20°E, are all steeply dipping, and range in width between 0.5 and 3 m. Flow directions for the dikes were determined by the bearing and plunge of the K_{max} (maximum principal susceptibility) axes relative to the dike orientation. About 66% of the dikes sampled show typical dike AMS patterns with K_{max} and K_{int} in the plane of the dike and K_{min} normal to the dike plane. About 66% of the dikes sampled have K_{max} inclinations $>45°$ and thus were emplaced upward; 16% of the dikes have K_{max} inclinations of $<10°$ and thus were emplaced laterally. The remaining dikes have intermediate K_{max} inclinations. With numerous dikes showing vertical to sub-vertical emplacement directions and with no magmatic source immediately below the detachment the dikes must predate emplacement of the upper plate. Therefore, upper plate dilation by dike intrusion could not be a driving force for protracted extension. Our date is consistent with a single catastrophic emplacement event, and inconsistent with an extensional allochthon model of incremental emplacement over long intervals of time.

Keywords: Anisotropy of magnetic susceptibility; Heart Mountain Detachment; Mafic dikes

1. Introduction

1.1. Overview of the Heart Mountain problem

Since first published reports of 'considerable confusion' at Heart Mountain by G.H. Eldridge (1894), the Heart Mountain Detachment (HMD) has been regarded as one of the most enigmatic features in North American structural geology (Fig. 1). The entire HMD area has been mapped previously at a scale of 1:62,500 (Pierce, 1965, 1966, 1970; Pierce and Nelson, 1968, 1969, 1971; Pierce et al., 1973, 1982). The major characteristics of the HMD as summarized by Pierce (1973) and Hauge (1990) are: (1) a dispersed (>3400 km^2 in area) upper plate consisting of dozens of mountain-sized (and many hundreds of smaller) occurrences, some of which were transported at least 50 km; (2) a detachment horizon that consistently occurs along a lower Ordovician bedding plane; (3) an average dip of the detachment horizon at the time of emplacement of less than 2°; (4) overall transport to the southeast; and (5) breakaway, bedding plane, and ramp components, with a younger-over-older age relation in the proximal area and an older-over-younger age relation in the distal area. The emplacement of the upper plate of the HMD was contemporaneous with widespread igneous activity in the Absaroka volcanic province. Eocene volcanic rocks of the Absaroka Volcanic Supergroup (Smedes and Prostka, 1972) currently overlie and fill some horizontal gaps between the allochthonous Paleozoic rocks. Hauge (1993) provides an excellent summary of the history of research, and the present points of controversy.

Two fundamentally different models describing the geometry, kinematic pattern, and emplacement of the

* Corresponding author. Tel.: +1 309 438 2692; fax: +1 309 438 5310.
E-mail address: dhmalon@ilstu.edu (D.H. Malone).

0191-8141/$ - see front matter © 2005 Elsevier Ltd. All rights reserved.
doi:10.1016/j.jsg.2005.09.002

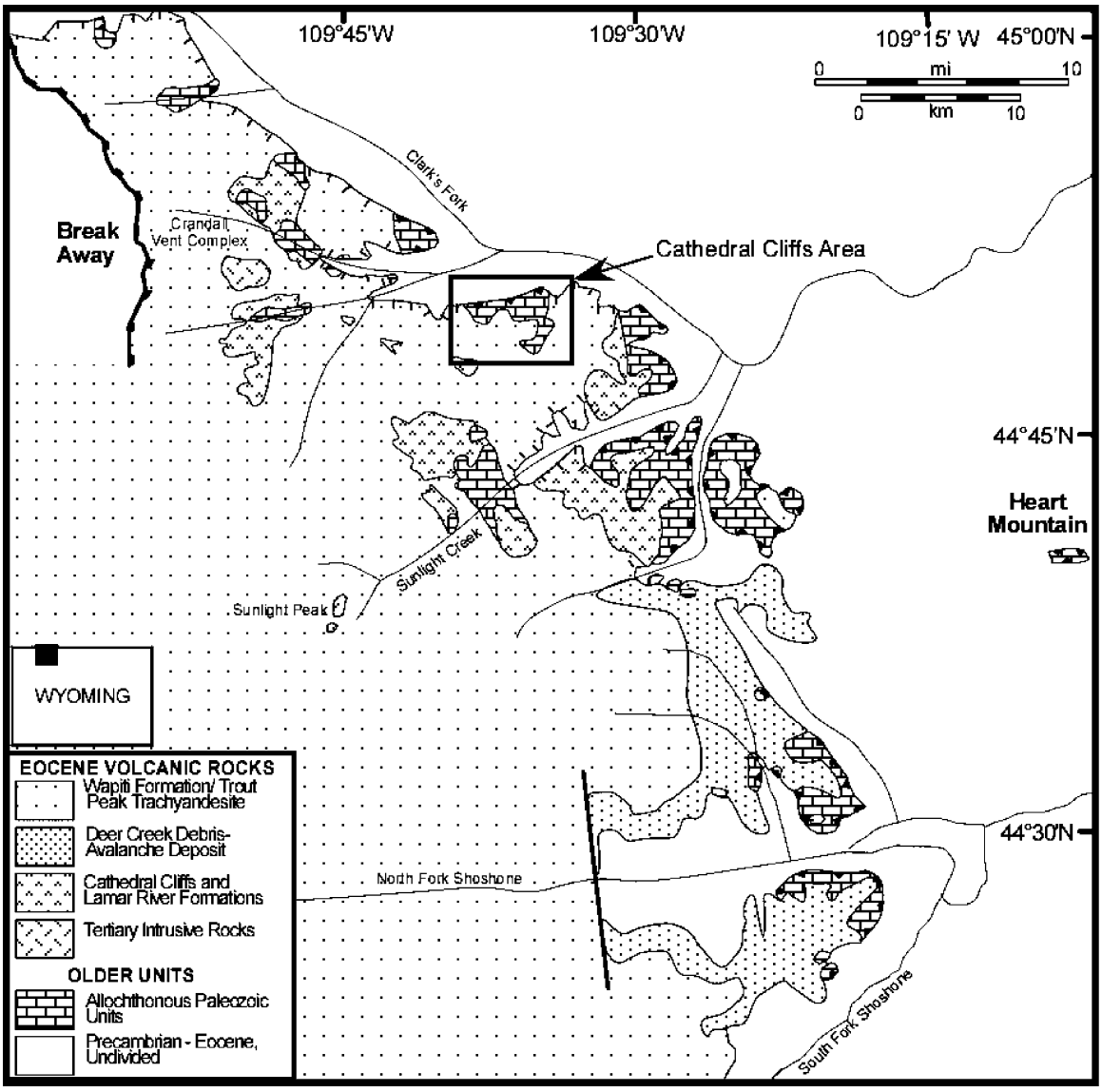

Fig. 1. Generalized geologic map of the Heart Mountain Detachment area (modified from Pierce (1987) and Malone (1995)).

upper plate of the HMD have been proposed. For many years, the upper plate was viewed to have been emplaced catastrophically as numerous independent slide blocks (Bucher, 1933; Pierce, 1957, 1973, 1987), and as a result of this detachment faulting, a tectonically denuded surface was formed. Immediately after faulting had ceased, massive outpourings of Wapiti Formation volcanic rocks were deposited on the detached blocks as well as on the tectonically denuded surface (Pierce, 1973, 1987). The most compelling line of evidence for this interpretation is the complete lack of erosion on the exposed fault plane, indicating that the time interval between slide block emplacement and the deposition of the Wapiti Formation must have been very short.

During the 1980s, a different model for the emplacement of the HMD allochthons was advanced. In this view, the upper plate is interpreted to have been a continuous allochthon rather than a series of individual slide blocks (Hauge, 1985, 1990, 1993). Volcanic rocks overlying the detachment, originally viewed as in depositional contact, were reinterpreted as involved in movement of the upper plate (Hauge, 1990). Thus, the continuous allochthon model requires no tectonic denudation or catastrophic emplacement of numerous slide blocks, and the model eliminates the mechanical enigma that tectonic denudation poses.

Recent reports on various aspects of the HMD can be found in Beutner and Craven (1996), Craddock et al. (2000), Malone (1995, 1996, 1997), Malone et al. (1999), Anders et al. (2000), and Rhodes et al. (in press).

1.2. Upper plate mafic dikes

The deposition and emplacement of associated Eocene volcanic rocks was accompanied by the intrusion of mafic

and intermediate dikes. These dikes commonly radiate from the volcanic centers near Crandall Creek and Sunlight Peak (Nelson et al., 1980). Many hundreds of dikes intrude the upper plate of the HMD, but only a few lower plate dikes have been reported (Hauge, 1985). One of the more spectacular dike swarms is at Cathedral Cliffs (Pierce, 1963b) (Figs. 2 and 3). Here, the dikes intrude both Paleozoic and overlying volcanic rocks. Pierce (1963b, 1987) and Hauge (1985) interpret these upper plate dikes to be laterally injected. According to Hauge (1985) "Dikes accommodate significant extension that is restricted to the upper plate, and syntectonic lateral intrusion from volcanic centers seems likely".

Pierce (1987) argues that they post-date movement. This interpretation was to preserve his two-fold explanation of upper plate emplacement: movement of the upper plate with some volcanic rocks and accompanying tectonic denudation, followed by burial by outpourings of Wapiti volcanic rocks. Because many of these dikes cut Paleozoic and the overlying volcanic rocks, but are not also found in the lower plate, they must be younger than and unrelated to faulting.

Hauge (1990) states that this is unlikely, because extension of the allochthon and attendant movement along the detachment are required to make the volume that the dikes occupy. Furthermore, Hauge (1993) states "A small but significant amount of extension of the allochthon is accommodated by igneous dikes related to Absaroka volcanism." Thus previous workers all interpret these dikes to be laterally intruded, but disagree as to the time of intrusion and kinematic significance with respect to the emplacement of the upper plate.

Although lateral intrusion of dikes has been assumed by most previous workers, no rigorous study of dike intrusion kinematics has been attempted. Our goal at Cathedral Cliffs was to investigate the emplacement kinematics of a number of mafic dikes using standard anisotropy of magnetic susceptibility (AMS) techniques to determine dike magnetic fabrics, which can be used as a proxy for emplacement direction. Thus, this research provides an important test of the lateral injection hypothesis, which is an essential component of each of the competing models for Heart Mountain faulting.

2. Geology of Cathedral Cliffs

The spectacular exposures at Cathedral Cliffs (Figs. 2 and 3) form part of a large allochthonous Paleozoic body that extends 5 km eastward from Corral Creek to just west of Reef Creek. The Paleozoic block is structurally complex; it is cut by many normal faults and trachyandesite dikes (Fig. 4; Kirchner, 1962; Pierce, 1963b; Pierce and Nelson, 1971; Hauge, 1985, 1990). Both the normal faults and igneous dikes are truncated downward at the bedding plane detachment fault (Fig. 4). The dikes range in thickness from 1 to 3 m in width, trend generally north–south and dip steeply (Figs. 5 and 6).

Above the allochthonous Paleozoic rocks, Pierce (1963a) defined the volcanic Cathedral Cliffs Formation; as much as 400 ft (125 m) of the unit is exposed here. Above the Cathedral Cliffs Formation, a succession in excess of 800 ft (250 m) in thickness of the Wapiti Formation is exposed. At this locality, the Wapiti Formation is crudely bedded, and it consists dominantly of vent and proximal-facies breccias. The stratigraphic relations in this area are further complicated by the presence of the Windy Mountain vent-complex, a relatively small vent-complex with a wide variety of intrusive rock types (Kirchner, 1962). Hauge (1990) suggested that this stratigraphic nomenclature be

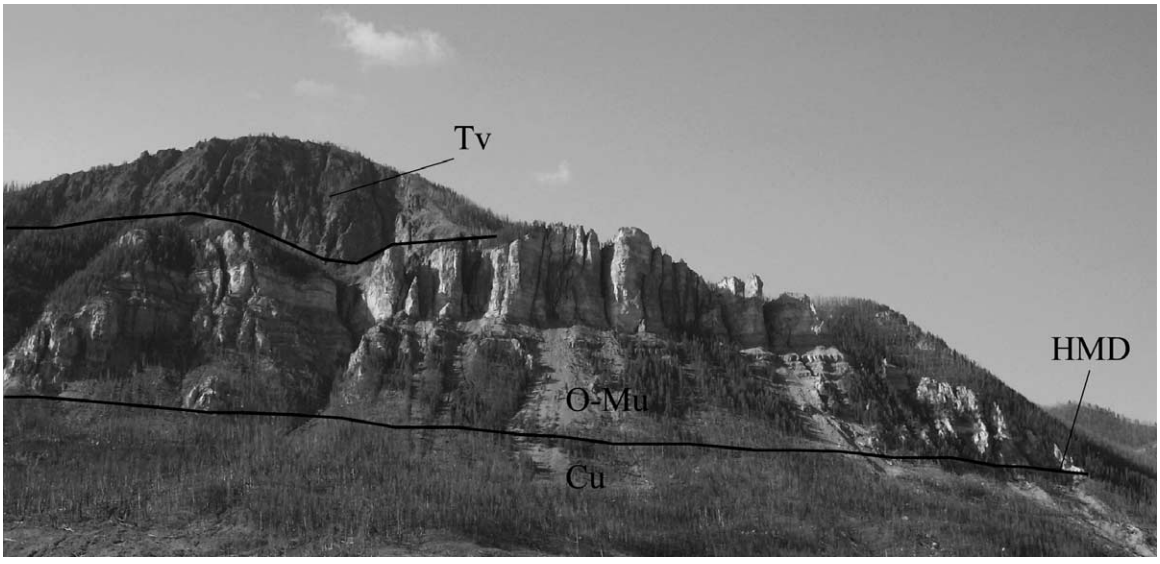

Fig. 2. Photo showing north face of Cathedral Cliffs; Cu, Autochthonous Cambrian rocks, undivided; O–Mu, Allochthonous Ordovician–Mississippian rocks, undivided; Tv, Tertiary volcanic rocks; HMD, Heart Mountain Detachment.

Fig. 3. Photo showing dikes intruding allochthonous Ordovician–Mississippian carbonate rocks.

abandoned. We found that at Cathedral Cliffs, the two-fold classification scheme to be appropriate.

The intrusive rocks at Cathedral Cliffs are most likely associated with volcanic/plutonic activity at the extensively eroded Sunlight Peak vent complex 20 km to the south. Magmatism at Sunlight Peak began at 49.6 Ma and concluded at 48.1 Ma (Feeley and Cosca, 2003). Sunlight Peak is in the eastern 'high-K' belt, where shoshonitic compositions dominate (Chadwick, 1970). Some dikes, especially those close to Sunlight Peak, have undergone hydrothermal alteration and contain secondary calcite (Feeley and Cosca, 2003). The least altered dikes were sampled for AMS analysis. They include as much as 30% phenocrysts of plagioclase, olivine, and pyroxene. A detailed geochemical and isotopic study of the dikes studied here is ongoing, and will be the subject of a future report.

3. Anisotropy of magnetic susceptibility

Anisotropy of magnetic susceptibility (AMS) is a technique commonly applied to igneous materials, particularly mafic dikes, as a proxy for magmatic flow (Ellwood, 1978; Knight and Walker, 1988; Park et al., 1988; Ernst,

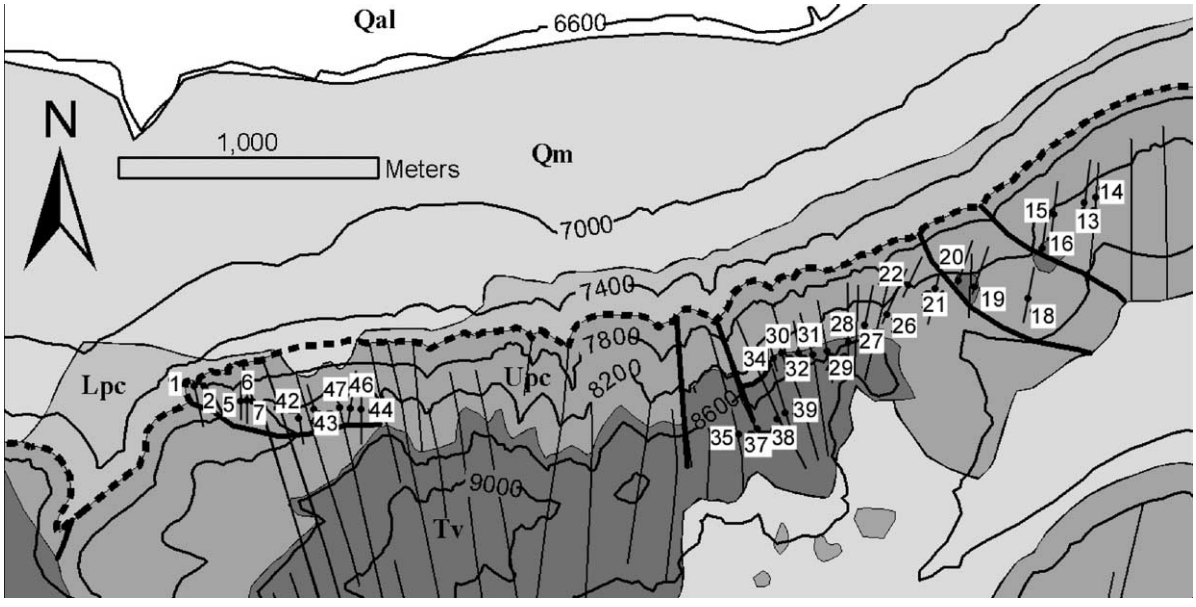

Fig. 4. Geologic map of Cathedral Cliffs showing sample localities. Modified from Pierce and Nelson (1971).

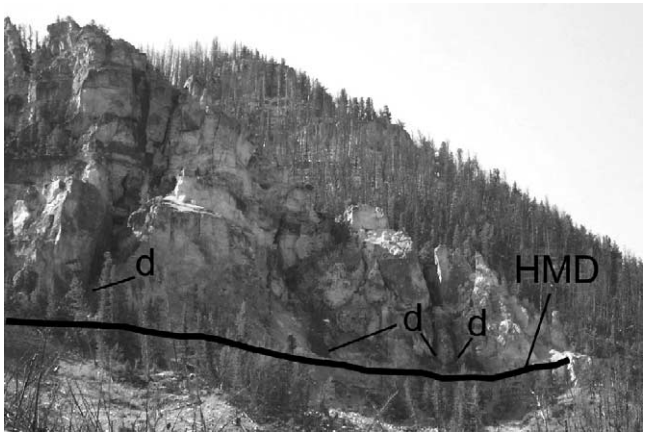

Fig. 5. Photo showing dikes (d) truncated along the Heart Mountain Detachment (HMD).

1990; Cadman et al., 1992; Puranen et al., 1992; Bates and Mushayandebvu, 1995; Raposo, 1997). AMS is defined as the variation in direction of the principal magnetic susceptibility axes within a rock sample. AMS fabric has been used to interpret flow direction in intrusive rocks and lava flows as well as interpreting major stress directions in metamorphosed rocks. AMS exposes the subtle fabrics of aligned magnetic crystals that are not observable using any imaging techniques.

In dikes, the orientation of the K_{max} axes can be used to infer the flow direction of the magma (Bates and Mushayandebvu, 1995). Magnetic susceptibility (K) for rocks is defined as

$$J = KH$$

where H is the applied magnetic field (A/m) and J is the induced magnetization (A/m). If K is anisotropic, it can be represented in space by the three principal axes K_{max}, K_{int}, and K_{min} of the magnitude ellipsoid (Hrouda, 1982). The shape of the magnitude ellipsoid is given by the anisotropy degree (P), which is defined as

$$P = K_{max}/K_{min}$$

where K_{max} and K_{min} are the values of the principal axes and the shape factor (T) defined as

$$T = \ln(F) - \ln(L)/\ln(F) + \ln(L)$$

where F is the foliation (K_{int}/K_{min}) and L is the lineation (K_{max}/K_{int}) of the magnitude ellipsoid. The shape factor ranges from -1 for a prolate ellipsoid to $+1$ for an oblate ellipsoid.

The shape and alignment of the magnitude ellipsoid represents the preferred alignment of ferromagnetic crystals during the emplacement of a magma body or crystal growth or realignment in a stress field (Ellwood, 1978). Magma flow is assumed to be an incompressible Newtonian fluid and governed by laminar flow (Shaw and Swanson, 1974), whereby prolate ellipsoids should align their long axes normal to the flow direction (Jeffery, 1922) and oblate ellipsoids will align their short axes normal to flow direction (Happel and Brenner, 1965). With these two particle behaviors combined, the intermediate axes will align themselves parallel to the flow direction (Bates and Mushayandebvu, 1995). Khan (1962) found that the magnitude ellipsoid shape conforms to the physical shape of magnetite grains, with the K_{max} axes representing the long axis of the grains, and that the K_{int} axes and the shape axes align themselves in the direction of magma emplacement. Magnetite crystals can become imbricated and become inclined as much as 30° near the dike margin (Knight and Walker, 1988). AMS fabrics may become isotropic or distorted due to degassing, oxidation, or continued crystallization (Sparks et al., 1977; Ellwood, 1978).

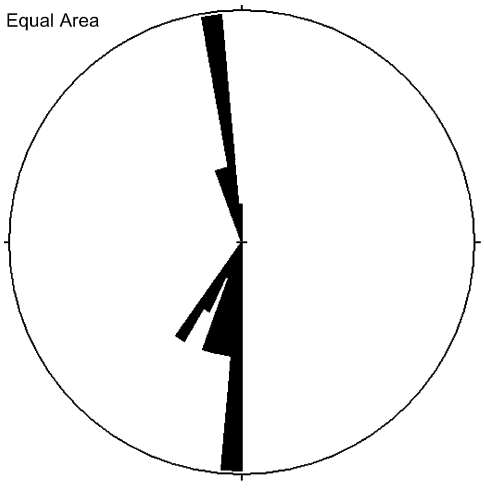

Fig. 6. Rose diagram showing strike and dip of sampled dikes. $n = 32$; outer circle 19%; mean direction 214.6°; $\alpha 95 = -1.0$.

4. Methodology

Thirty-two block samples were collected from the field and oriented using a brunton compass (Fig. 6). One block sample was collected and analyzed for each dike. Because of precipitous slopes and steep climbs, access to dikes that occur along the basal detachment was not possible. The sample locations are provided in Fig. 4. Samples were taken from the middle of the exposed dike where possible and only a few were taken from the dike margin. Highly weathered intervals were avoided. Samples were collected from dikes that intrude the Paleozoic carbonate rocks as well as the overlying Tertiary volcanic rocks. Samples were slabbed along the horizontal surface and then drilled into about 20, 1.65 cm by 1.65 cm cylindrical cores each.

The 'Roly-Poly' is an AC susceptibility bridge with an automated sample handler for determining anisotropy of low-field magnetic susceptibility at room temperature, and is housed at the Institute for Rock Magnetism at the University of Minnesota. An alternating current in the

external 'drive' coils produces an alternating magnetic field in the sample space with a frequency of 680 Hz and an amplitude of up to 1 mT. The induced magnetization of a sample is detected by a pair of 'pickup' coils, with a sensitivity of 1.2×10^{-6} SI volume units. For anisotropy determination, a sample is rotated about three orthogonal axes, and susceptibility is measured at 1.8° intervals in each of the three measurement planes. The susceptibility tensor is computed by least squares from the resulting 600 directional measurements. High precision results from the large number of measurements; in most cases principal axis orientations are reproducible to within two degrees, and axial ratios to within about 1%. For each measured cube or core, one unique magnitude ellipsoid is produced.

5. Results

The structural characteristics and magnetic fabric information of the dikes are provided in Tables 1 and 2. Mean susceptibilities (K) of the 32 dikes sampled range from 1.972×10^{-2} to 4.727×10^{-2} SI with an arithmetic mean of 3.201×10^{-2} SI. The anisotropy degree (P) for the dikes ranged from 1.005 to 1.184 with a mean of 1.039 or 3.9%. With some rather low anisotropy degrees in some of the samples, one sample was tested using the kappa bridge instrument, which produces more accurate data than that of the Roly-Poly on samples with anisotropy degrees less than 2%. The mean susceptibility directions determined using the kappa bridge are consistent with the directions obtained using the Roly-Poly, so the authors are confident with data produced by the Roly-Poly on samples with low anisotropy degrees.

Three cores from 18 of the samples were analyzed using a vibrating sample magnetometer (VSM) at the IRM to determine the minerals responsible for the AMS fabric. The hysterisis parameters J_{rs}/J_s (remanence/saturation remanence) and H_{cr}/H_c (coercivity of remanence/coercive force) derived from the VSM were used (Day et al., 1977; Dunlop, 1986) to better determine whether the magnetite fell into the single domain (SD), pseudo-single domain (PSD), or multi-domain (MD) range. As shown in Fig. 7, most of the samples fall into the MD range, with a few in the PSD range and no samples falling into the SD range. This means that

Table 1
AMS parameters for the dikes sampled at Cathedral Cliffs

Sample	No. of cores	$K\times10^{-2}$ SI	SD of K	P (K_{max}/K_{min})	L (K_{max}/K_{int})	F (K_{int}/K_{min})	T (ln F−ln L)/(ln F+ln L)
CC0401	20	3.369	0.263	1.038	1.009	1.029	0.523
CC0402	12	3.147	0.494	1.019	1.013	1.006	−0.367
CC0405	20	3.171	0.291	1.025	1.019	1.006	−0.518
CC0406	20	4.228	0.401	1.033	1.012	1.021	0.271
CC0407	20	3.782	0.356	1.031	1.013	1.018	0.160
CC0413	20	3.633	0.225	1.043	1.019	1.024	0.115
CC0414	16	3.686	0.264	1.012	1.005	1.007	0.166
CC0415	12	2.692	0.164	1.033	1.023	1.010	−0.391
CC0416	19	2.302	0.283	1.048	1.009	1.039	0.620
CC0418	9	3.667	0.210	1.038	1.025	1.013	−0.313
CC0419	15	2.906	0.150	1.050	1.007	1.042	0.710
CC0420	15	1.972	0.222	1.035	1.012	1.023	0.312
CC0421	10	3.215	3.050	1.022	1.021	1.001	−0.908
CC0422	17	2.526	0.218	1.030	1.016	1.013	−0.103
CC0426	18	2.930	0.300	1.019	1.014	1.004	−0.554
CC0427	10	3.225	0.215	1.035	1.002	1.034	0.887
CC0428	11	3.049	0.170	1.042	1.015	1.027	0.283
CC0429	19	3.568	0.313	1.015	1.006	1.007	0.077
CC0431	14	2.635	0.141	1.016	1.012	1.004	−0.499
CC0432	12	2.943	0.290	1.039	1.019	1.020	0.025
CC0433	21	2.769	0.100	1.005	1.002	1.003	0.200
CC0434	13	2.699	0.154	1.086	1.013	1.072	0.687
CC0435	19	2.959	0.317	1.024	1.013	1.011	−0.083
CC0437	13	3.152	0.306	1.044	1.027	1.016	−0.253
CC0438	9	3.108	0.096	1.045	1.024	1.021	−0.066
CC0439	14	4.433	0.219	1.044	1.003	1.041	0.861
CC0440	20	3.687	0.213	1.043	1.001	1.043	0.954
CC0442	10	3.574	0.293	1.018	1.006	1.012	0.332
CC0443	17	2.986	0.203	1.011	1.003	1.008	0.454
CC0444	15	2.331	0.132	1.184	1.045	1.133	0.479
CC0446	17	4.727	0.460	1.029	1.009	1.020	0.377
CC0447	17	3.351	0.199	1.081	1.039	1.041	0.025

sK, bulk susceptibility; SD of K, standard deviation of the bulk susceptibility; P, anisotropy degree; L, lineation; F, foliation; T, shape factor.

Table 2
Sample location and the mean directions for the principal susceptibility axes

Sample	UTM		Strike	K_{max}				K_{int}				K_{min}				Fabric
	X	Y		Dec (°)	Inc (°)	Ma (°)	ma (°)	Dec (°)	Inc (°)	Ma (°)	ma (°)	Dec (°)	Inc (°)	Ma (°)	ma (°)	
CC0401	609810	4964330	N10W	99.6	9.1	2.9	1.4	190.7	6.8	1.5	2.9	317.1	78.6	1.1	1.8	III
CC0402	609844	4964330	N16W	52.3	40.2	5.0	3.0	285.7	35.2	11.9	4.1	171.6	30.1	3.2	11.8	IVa
CC0405	610021	4964260	N–S	157.8	59.7	2.3	3.1	64.4	2.0	5.4	2.2	333.2	30.2	3.0	5.3	IIa
CC0406	610024	4964260	N–S	11.0	10.2	2.4	1.8	102.6	8.8	2.0	2.2	232.7	76.5	2.7	1.3	IIb
CC0407	610027	4964260	N–S	186.4	5.0	2.1	0.7	91.1	46.9	3.1	1.8	281.0	42.6	0.8	3.0	IVb
CC0413	613290	4965039	N26E	2.0	58.1	2.8	0.6	197.3	30.9	0.8	2.8	103.2	6.9	0.6	0.8	Ia
CC0414	613293	4965039	N20E	143.9	76.4	4.8	2.5	34.2	4.7	303.2	12.8	303.2	12.8	2.5	2.6	Ia
CC0415	613138	4964981	N15E	21.1	77.0	2.5	4.3	188.5	12.7	4.8	3.5	279.1	2.7	1.6	5.8	Ia
CC0416	613096	4964863	N10E	35.4	72.2	3.0	0.7	193.6	16.6	0.9	3.0	285.4	6.3	0.7	0.9	Ia
CC0418	613032	4964662	N10E	341.9	81.4	7.9	5.2	195.3	7.2	4.9	9.6	104.7	4.7	4.5	7.9	Ia
CC0419	612810	4964700	N15E	9.0	53.0	12.1	1.5	178.2	36.6	1.0	12.1	272.1	5.2	1.6	1.0	Ia
CC0420	612788	4964700	N30E	16.1	2.1	5.3	1.0	280.4	69.6	2.1	5.3	106.9	20.3	1.0	2.3	Ib
CC0421	612658	4964709	N10E	14.1	77.8	6.2	1.7	220.9	11.0	38.1	4.7	129.8	5.4	4.3	38.1	Ia
CC0422	612587	4964709	N30E	67.3	73.7	2.6	1.3	191.3	9.3	1.6	2.6	283.5	13.3	1.3	1.8	Ia
CC0426	612459	4964569	N25E	341.4	67.5	5.8	2.1	152.0	22.2	14.1	5.5	243.3	3.3	2.4	14.1	IVa
CC0427	612416	4964549	N15E	10.8	39.2	45.1	1.6	191.3	50.3	2.8	45.1	101.0	0.2	1.8	4.7	Ia
CC0428	612275	4964469	N–S	200.5	78.5	5.3	2.2	21.5	11.5	1.2	5.3	291.4	0.2	2.3	1.1	Ia
CC0429	612247	4964465	N15W	4.8	54.2	3.9	2.0	170.5	35.0	3.2	4.0	265.3	6.8	1.8	3.5	Ia
CC0431	612202	4964446	N20W	16.2	23.4	5.4	2.1	235.4	60.9	9.5	5.1	113.5	16.4	2.2	9.4	Ib
CC0432	612128	4964455	N10W	25.6	82.3	3.7	1.7	169.6	6.3	1.6	3.7	260.1	4.5	2.2	0.8	Ia
CC0433	612086	4964443	N10W	43.8	63.9	21.5	4.8	246.0	24.4	9.9	21.8	152.0	8.7	4.4	10.8	IIa
CC0434	612066	4964443	N30E	14.7	57.6	4.5	0.8	182.8	31.1	0.5	4.4	276.2	5.4	0.9	0.4	Ia
CC0435	611916	4964141	N10W	6.5	4.5	3.2	1.1	112.8	74.4	4.3	2.0	275.3	14.9	1.1	3.6	Ib
CC0437	611993	4964161	N5E	333.2	80.3	2.8	1.5	199.3	6.8	3.2	2.5	108.4	6.9	1.4	3.0	Ia
CC0438	612086	4964203	N10W	141.4	78.6	3.4	1.3	331.6	11.2	1.7	3.2	241.2	1.9	2.2	1.2	Ia
CC0439	612085	4964202	N15W	266.9	79.1	16.2	2.3	156.2	3.9	2.2	16.2	65.5	10.2	1.4	2.9	Ia
CC0440	609938	4964381	N5E	10.9	10.6	29.0	0.3	226.8	77.0	0.9	29.0	102.3	7.4	0.3	0.9	Ib
CC0442	610228	4964203	N5W	66.4	58.8	12.6	1.5	301.5	19.1	4.2	12.7	202.7	23.7	1.4	4.5	IVa
CC0443	610283	4964238	N10W	32.9	45.1	18.0	4.0	188.7	42.2	6.2	18.0	290.2	12.4	3.9	6.3	Ia
CC0444	610454	4964238	N–S	268.3	5.9	1.4	0.9	174.2	34.2	0.6	1.7	6.9	55.2	0.9	1.1	III
CC0446	610437	4964238	N5E	237.5	67.7	7.3	1.8	56.4	22.3	2.0	7.3	146.5	22.3	1.9	2.1	IVa
CC0447	610407	4964244	N–S	245.5	17.0	1.3	0.6	149.5	18.9	1.0	1.2	14.7	64.1	0.7	1.0	III

Dec, declination of the given *K*-axis; Inc, inclination of the given *K*-axis; Ma and ma, major and minor semiangles of the 95% confidence ellipse, respectively.

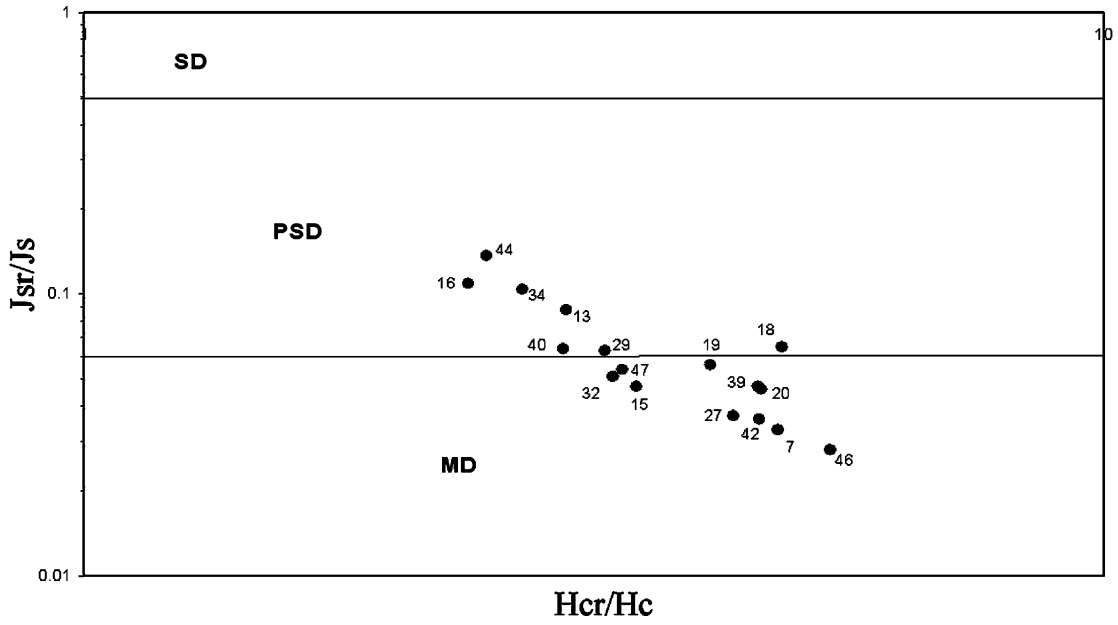

Fig. 7. Plot of J_{rs}/J_s (remanence/saturation remanence) versus H_{cr}/H_c (coercivity of remanence/coercive force) or hysteresis ratios of 18 dikes sampled at Cathedral Cliffs (after Day et al., 1977), with the fields for single domain (SD), pseudo-single domain (PSD), and multi-domain (MD) magnetite (values taken from Dunlop (1986)).

there is no inverse AMS fabric present in any of the dikes sampled, where K_{min} represents the long axis in the grains.

Mean susceptibility directions for each of the 32 dikes sampled are shown in Fig. 8. Of the 32 dikes sampled, 21 of these show typical dike fabric (*I*), with the K_{max} and K_{int} axes lying in the plane of the dike and the K_{min} axes normal to the dike plane. Seventeen of these 21 dikes have K_{max} inclinations greater than 45° (Ia) and the remaining four have K_{max} inclinations less than 45° (Ib). Three dikes have a fabric (II) with the K_{max} and K_{min} axes in the plane of the dike and K_{int} normal to the dike plane. Two of these three dikes have their K_{max} axes greater than 45° (IIa) and the other has its K_{max} inclined 10° (IIb). Three dikes have their K_{int} and K_{min} axes in the plane of the dike and their K_{max}

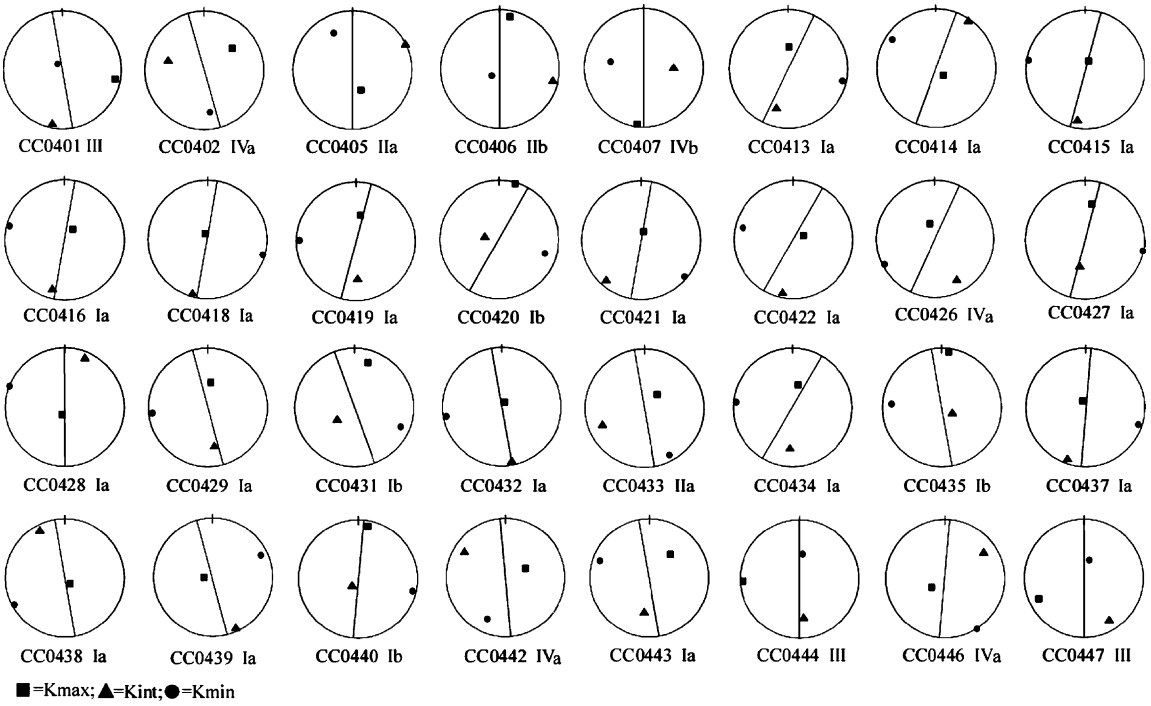

Fig. 8. Equal-area stereonets showing dike attitude and *K* vectors, with the interpreted fabric type.

axes normal to the dike plane and nearly horizontal (III). The remaining five dikes have anomalous fabrics (IV) with four having their K_{max} axes greater than 45° (IVa, IVb for the other). Overall, 66% of the dikes sampled have their K_{max} axes inclined greater than 45° and 16% have K_{max} axes inclined less than 10°.

6. Discussion and conclusions

These data indicate that the majority (>70%) of the igneous dikes sampled at Cathedral Cliffs have steep K_{max} vectors. It is doubtful that these dikes are kinematically related to the emplacement of the upper plate, as envisioned in the continuous allochthon model of Hauge (1990). Thus, dike intrusion as a means of accommodating a 'small but significant' component of the extension of the upper plate is not, at least at Cathedral Cliffs, a viable process.

It is also doubtful that they are younger than the emplacement of the upper plate, as envisioned by Pierce (1987) in terms of the tectonic denudation model. Pierce's argument for the late emplacement of the dikes was due largely to how he perceived the stratigraphic relationship of the dikes to the volcanic rocks which the dikes intrude. In Pierce's interpretation, some of the volcanic rocks were older than faulting (Cathedral Cliffs Formation), while others were younger than faulting (Wapiti Formation). Furthermore, he suggests that because some dikes terminate on the HMD, and extend upward through the entire volcanic succession, they must have been younger than faulting and thus laterally injected. Hauge (1985, 1990) argued convincingly that the volcanic stratigraphic nomenclature in the proximal areas of the HMD was problematic and should be abandoned. We concur with this recommendation.

The most reasonable explanation for these dikes is that they are older than faulting. This is a similar argument for the allochthonous plutonic rocks at White Mountain, about 10 km to the southeast. The roots of the dikes studied here are likely buried beneath younger volcanic rocks northwest or west of Cathedral Cliffs. It is possible and perhaps likely that dike intrusion occurred immediately prior to the emplacement of the upper plate, and that volcanic processes were involved in the emplacement event.

Some dikes (~20%) have gently inclined or flat K_{max} vectors, and likely were injected laterally. The relationship of these dikes to the emplacement of the upper plate cannot be determined with certainty. They can be coeval with emplacement, as interpreted by Hauge (1985, 1990), younger than emplacement (Pierce, 1987) or older than and unrelated to the emplacement event, as argued above. It is curious though, that virtually all dikes, no matter their emplacement direction, terminate along the HMD. This observation in itself leads to the obvious interpretation that the dikes are indeed older than faulting.

Acknowledgements

The authors would like to thank the Illinois State University's Honors Department and the Colorado Scientific Society's William G. Pierce Memorial Fund providing support for this research. We also appreciate the efforts of Mike Jackson, IRM, University of Minnesota, for his support with our laboratory analysis. Timothy B. Sickbert and Christopher Ball provided important assistance during the field phase of this investigation. Mark Anders and Martin Mushayandebvu provided helpful and constructive reviews.

References

Anders, M.H., Aharanov, E., Walsh, J.J., 2000. Stratified granular material beneath large slide blocks; implications for mode of emplacement. Geology 28, 971–974.

Bates, M.P., Mushayandebvu, M.F., 1995. Magnetic fabric in the Umvimeela Dyke, satellite of the Great Dyke, Zimbabwe. Tectonophysics 242, 241–254.

Beutner, E.C., Craven, A.E., 1996. Volcanic fluidization and the Heart Mountain detachment, WY. Geology 24, 595–598.

Bucher, W.H., 1933. Remarkable local folding, possibly due to gravity, bearing on the Heart Mountain thrust problem. Geological Society of America Proceedings 1935, 69.

Cadman, A.C., Park, R.G., Tarney, J., Halls, H.C., 1992. Significance of anisotropy of magnetic susceptibility fabrics in Proterozoic mafic dikes, Hopedale Block, Labrador. Tectonophysics 207, 303–314.

Chadwick, R.A., 1970. Belts of eruptive centers in the Absaroka–Gallatin volcanic province, Wyoming-Montana. Geological Society of America Bulletin 81, 267–274.

Craddock, J.P., Neilsen, K.J., Malone, D.H., 2000. Calcite twinning strain constraints on the hearth mountain detachment emplacement rates and kinematics. Journal of Structural Geology 22, 983–991.

Day, R., Fuller, M., Schmidt, V.A., 1977. Hysterisis properties of titanomagnetites: grain size and compositional dependence. Physics of Earth and Planetary Interiors 13, 260–267.

Dunlop, D.J., 1986. Hysteresis properties of magnetite and their dependence on particle size: a test of the pseudo-single-domain remanence models. Journal of Geophysical Research 91, 9569–9584.

Eldridge, G.H., 1894. A geological reconnaissance in northwest Wyoming. US Geological Survey Bulletin 110, 30–31.

Ellwood, B.B., 1978. Flow and emplacement direction determined for selected basaltic bodies using magnetic susceptibility anisotropy measurements. Earth and Planetary Science Letters 41, 254–264.

Ernst, R.E., 1990. Magma flow directions in two mafic Proterozoic dike swarms of the Canadian Shield: as estimated using anisotropy of magnetic susceptibility. In: Parker, A.J., Rickwood, P.C., Tucker, D.H. (Eds.), Mafic Dikes and Emplacement Mechanisms. Balkema, Rotterdam, pp. 231–235.

Feeley, T.C., Cosca, M.A., 2003. Time vs. composition trends of magmatism at Sunlight Volcano, Absaroka Volcanic Province, Wyoming. Geological Society of America Bulletin 115, 714–728.

Happel, J., Brenner, H., 1965. Low Reynolds Number Hydrodynamics. Prentice Hall, Englewood Cliffs, NJ. 553pp.

Hauge, T.A., 1985. Gravity-spreading origin of the Heart Mountain Allochthon, northwestern Wyoming. Geological Society of America Bulletin 96, 1440–1456.

Hauge, T.A., 1990. Kinematic model of a continuous Heart Mountain allochthon. Geological Society of America Bulletin 102, 1174–1188.

Hauge, T.A., 1993. The Heart Mountain detachment, northwestern

Wyoming: 100 years of controversy. In: Snoke, A.W., Steidtman, J.R., Roberts, S.M. (Eds.), Geology of Wyoming Geological Survey Memoir, 5, pp. 530–571.

Hrouda, F., 1982. Magnetic anisotropy of rocks and its application in geology and geophysics. Geophysical Surveys 5, 37–82.

Jeffery, G.B., 1922. The motion of ellipsoidal particles immersed in a viscous fluid. Proceedings of the Royal Society of London, Series A 102, 161–179.

Khan, M.A., 1962. The anisotropy of magnetic susceptibility of some igneous and metamorphic rocks. Journal of Geophysical Research 67, 2873–2885.

Kirchner, J.G., 1962, The Geology of the Windy Mountain Area, Park County Wyoming. MS Thesis, Wayne State University.

Knight, M.D., Walker, G.P.L., 1988. Magma flow directions in dikes of the Koolau Complex, Oahu, determined from magnetic fabric studies. Journal of Geophysical Research 93, 4301–4319.

Malone, D.H., 1995. A very large debris-avalanche deposit within the Eocene volcanic succession of the Northeasten Absaroka Range, Wyoming. Geology 23, 661–664.

Malone, D.H., 1996. Revised stratigraphy of Eocene volcanic rocks in the Lower North and South Fork Shoshone River Valleys, Wyoming. Wyoming Geological Association Annual Field Conference Guidebook 47, 109–138.

Malone, D.H., 1997. Recognition of a distal facies greatly extends the domain of the Deer Creek Debris–Avalanche Deposit (Eocene), Absaroka Range, Wyoming. Wyoming Geological Association Annual Field Conference Guidebook 48, 1–9.

Malone, D.H., Hauge, T.A., Beutner, E.L., 1999. Field guide for the Heart Mountain detachment and associated structure. Geological Society of America Field Guide 1, 177–203.

Nelson, W.H., Prostka, H.J., Williams, F.E., 1980. Geology and mineral resources of the North Absaroka Wilderness and vicinity, Park County, Wyoming. United States Geological Survey Bulletin 1447, 101.

Park, J.K., Tanczyk, E.I., Desbarats, A., 1988. Magnetic fabric and its significance in the 1400 Ma Mealy diabase dikes of Labrador, Canada. Journal of Geophysical Research 93, 13,689–13,704.

Pierce, W.G., 1957. Heart Mountain and South Fork detachment thrusts of Wyoming. American Association of Petroleum Geologists Bulletin 41, 591–626.

Pierce, W.G., 1963a. Cathedral Cliffs Formation, the early acid breccia unit of northwestern Wyoming. Geological Society of America Bulletin 74, 9–22.

Pierce, W.G., 1963b. Reef Creek detachment fault, northwest Wyoming. Geological Society of America Bulletin 74, 1225–1236.

Pierce, W.G., 1965. Geologic map of the Deep Lake Quadrangle, Park County, Wyoming. US Geological Survey Quadrangle Map GQ-477, scale: 1:62,500.

Pierce, W.G., 1966. Geologic map of the Cody Quadrangle. Park County, Wyoming. US Geological Survey Quadrangle Map GQ-542, scale: 1: 62,500.

Pierce, W.G., 1970. Geologic map of the Devil's Tooth quadrangle. Park County, Wyoming. US Geological Survey Quadrangle Map GQ-755, scale: 1:62,500.

Pierce, W.G., 1973. Principal features of the Heart Mountain fault and the mechanism problem. In: DeJong, K. (Ed.), Gravity and Tectonics. Wiley, New York, pp. 457–471.

Pierce, W.G., 1987. The case for tectonic denudation by the Heart Mountain Fault; a response. Geological Society of America Bulletin 99, 552–568.

Pierce, W.G., Nelson, W.H., 1968. Geologic map of the Pat O'Hara quadrangle, Park County, Wyoming. US Geological Survey Quadrangle Map GQ-755, scale: 1:62,500

Pierce, W.G., Nelson, W.H., 1969. Geologic map of the Wapiti quadrangle. Park County, Wyoming. US Geological Survey Quadrangle Map GQ-778, scale 1:62,500.

Pierce, W.G., Nelson, W.H., 1971. Geologic map of the Beartooth Butte quadrangle. Park County, Wyoming. US Geological Survey Quadrangle Map GQ-935, scale: 1:62,500.

Pierce, W.G., Nelson, W.H., Prostka, H.J., 1973. Geologic map of the Pilot Peak Quadrangle. Park County, Wyoming. US Geological Survey Report of Miscellaneous Investigations, I-816, scale: 1:62,500

Pierce, W.G., Nelson, W.H., Prostka, H.J., 1982. Geologic map of the Dead Indian Peak Quadrangle, Park County, Wyoming. US Geological Survey Quadrangle Map GQ-1564, scale: 1:62,500.

Puranen, R., Pesonen, L.J., Pekkarinen, L.J., 1992. Interpretation of magnetic fabrics in the Early Proterozoic diabase dikes of Keurau, central Finland. Physics of Earth and Planetary Interiors 72, 68–88.

Raposo, M.I.B., 1997. Magnetic fabric and its significance in the Florianopolis dyke swarm, southern Brazil. Geophysical Journal International 131, 159–170.

Rhodes, M.K., Malone, D.H., Carrol, A.R., Smith, M. (in press). Sudden Desiccation of Ancient Lake Gosiute at 49 Ma: A Downstream Effect of Heart Mountain Faulting? Paper to be published in a Wyoming Geological Survey Memoir on the Green River Basin.

Shaw, H.R., Swanson, D.A., 1974. Eruption flow rates of flood basalts. Proceedings of the Second Colombia River Basalt Symposium, 271–299.

Smedes, H.W., Prostka, H.J., 1972. Stratigraphic framework of the Absaroka Volcanic Supergroup in the Yellowstone Park Region. United States Geological Survey Professional Paper 729C, 33.

Sparks, R.S.J., Pinkerton, H., MacDonald, R., 1977. The transport of xenoliths in magmas. Earth and Planetary Science Letters 35, 234–238.